MODELLING INTERNAL STRUCTURE OF ASTEROIDS VIA DATA-DRIVEN APPROACH

Yuying Liang[1], Naoya Ozaki[2], Yasuhiro Kawakatsu[3], Masaki Fujimoto[4]

1 Introduction

The homogenous density distribution is not a proper approximation for asteroids that have undergone differentiation, which is demonstrated by iron meteorites analogous to planetary cores and stony achondrites analogous to crusts (Scheinber et al. 2015). The possible end-states of asteroid differentiation are either partially or fully differentiated body, or being disrupted into a rubble pile (Scheinberg et al. 2015). It is widely believed that some large asteroids like Ceres and Vesta are differentiated into a central mass core covered by a surface layer probably with mantle layer between them (Thomas et al. 2005, Zuber et al. 2011). The reflection spectrum of 21 Lutetia also supports its differentiated interior (Neumann et al. 2013, Neumann et al. 2018). These large asteroids are central to understanding planetary evolution and plays an important role in the simulation of the physical and chemical processes of terrestrial planet accretion (Zuber et al. 2011). The gravity field measurement is obtained from spacecraft-based tracking by a combination of Deep Space Network ranging and Doppler measurements with the onboard framing camera for optical imaging on the surface of the asteroids in real missions like Dawn (Konopliv et al. 2011) and OSRIS-REx (Scheeres et al. 2020). The optical measurements also provide flying data on the spacecraft location in the asteroid-centered body frame (Scheeres et al. 2020). This technical fact enlightens the authors by such question whether it is applicable to "read" the density distribution of asteroids directly from the spacecraft's flying state.

For this purpose, a mapping between two groups of data, i.e., the flying state of spacecraft and the density distribution of the target asteroid, must be established in this investigation and this dynamical link can not be explicitly expressed mathematically due to the strong nonlinearity of the real dynamical environment. For such complex problem, a family of machine learning techniques, named deep learning based on artificial neural networks (ANNs) is remarkably powerful for automatically creating the feature extractors using large amount of data (Goodfellow et al. 2016). As is pointed out by the universal approximation theorem (Nielsen 2015), ANNs are able to approximate an arbitrary function. Thus, ANNs approach is expected to construct a mapping between flying state observation and density distribution of asteroids. Among various applications by different ANN approaches, the unmatched dimension between the physical parameter space (the density distribution in this investigation) and the observation space (the flying state in this investigation) results in ambiguous problem because multiple parameter sets can result in the same observation (i.e., degeneracies). Classical neural networks can not address this ambiguity directly and failed to fully characterize degeneracies (Ksoll et al. 2020). However, so-called invertible neural networks (INNs) are well suited to cope with this difficulty (see Ardizzone et al. 2019a for instance). INNs learn the forward process after adding additional latent output variables to capture the information otherwise lost. This data-driven approach has been applied to determine the stellar parameter from photometry (Ksoll et al. 2020). Unfortunately, such unmatched dimension problem is to appear in this investigation for the parameterization of density distribution does not guarantee a physical parameter space that own equal dimension to the flying state observation, which is normally 6-dimensional. Besides this issue, the computation burden is exponentially increased for Monto Carlo simulation as one-more dimensional parameter is added to describe the density distribution. Thus, INNs are introduced in this investigation to construct the mapping between density distribution and flying state.

The summary of this investigation is organized as follows: In **Section 2**, a multiple-layer assumption is adopted to describe the internal structure of a differentiated asteroid and two nominal flying trajectories are chosen to offer flying state observations; In **Section 3**, the neural network is setup with the INNs architecture briefly introduced and the training

[1] Post-doctoral fellowship, Department of Solar System Science, ISAS/JAXA.
[2] Assistant Professor, Department of Space and Astronautical Science, ISAS/JAXA.
[3] Professor, Department of Space and Astronautical Science, ISAS/JAXA.
[4] Professor and deputy director general, Department of Solar System Science, ISAS/JAXA.

process is evaluated; In **Section 4**, the performances of the trained model are analyzed in two testing cases; key findings are summarized in **Conclusions**.

2 Astrophysical and Astrodynamical Environment Setup

2.1 Multiple-layered Internal Structure Model

A paramount example of fully differentiated asteroids is Vesta, which is taken as the target body of this investigation. Note that the methodology developed can also be applied to other differentiated celestial bodies. The internal structure of Vesta can be interpreted by a multiple-layered model consisting of core, mantle and crust for three-layer assumption or core and curst for two-layer assumption (Parker et al. 2014, Kattoum and Dombard 2008, etc), ignoring the slight local density deviation along the same layer. In this investigation, Vesta is approximated by two-layered structure using a combination of a single polyhedral and ellipsoids, respectively. Its surface characteristics are captured by the polyhedron. The core and mantle structures are represented by the ellipsoids, which is a widely used simplification in many literatures (Parker et al. 2014, Zuber et al. 2011, etc). Such two-layered model provides a satisfactory fit to gravity data alone while the three-layered mode is more appropriate for Vesta's interior considering the independent geochemical and petrological constrains (Parker et al. 2014).

Fig. 1 provides a sketch of two-layered structure of Vesta, where the internal section is colored by green and the polyhedral surface[5] is indicated by grey. The core modelled by an ellipsoid is indicated by dark green and its center coincides with the mass center of polyhedral Vesta. To mathematically describe the motion of a spacecraft around Vesta, a body-fixed rotating frame, denoted as O-x-y-z, is attached to the mass center of the Vesta body. The x-axis lies along the line from the Sun to Vesta at t=0 with the y-axis perpendicular to it, completing a right-handed coordinate system. The z-axis aligns the spin axis of Vesta. The three semi-major axes of the core ellipsoid, indicated by a_1, b_1, and c_1, aligns to the x, y, and z-axis, respectively. One more ellipsoid is added in order to upgrade to a three-layered model. Hence, the equations of motion of a spacecraft in the gravity field of multiple-layered structure of Vesta follow

$$\ddot{x}-2\omega\dot{y}=\frac{\partial\Omega}{\partial x},\ \ddot{y}+2\omega\dot{x}=\frac{\partial\Omega}{\partial y},\ \ddot{z}=\frac{\partial\Omega}{\partial z} \tag{1}$$

where ω denotes the spin rate of Vesta and taken as 1617.33 degree/day [6].

$$\Omega(x,y,z)=\frac{x^2+y^2}{2}\omega^2+U_{Vesta}(x,y,z) \tag{2}$$

where U_{Vesta} denotes the gravitational potential due to the Vesta body and can be approximated by the sum of each layer. For two-layered structure,

$$U_{Vesta}(x,y,z)=U_{crust}+U_{mantle} \tag{3}$$

where U_{crust} and U_{mantle} denotes the gravity potential due to the crust and the mantle, respectively.

Since the mantle is modelled by ellipsoids, a Ferrers' ellipsoid model (Ferrers 1870) is introduced to evaluate its potential and gravitational acceleration exerted upon the spacecraft (Bellerose and Scheeres 2007), which was used by the first author in (Liang et al. 2019). According to this model, the matter is uniformly distributed in the entire ellipsoid body and decreases smoothly to zero at its surface, so its gravity potential is explicitly expressed by the density and the size of the ellipsoid (Gómez 2007). Thus, the gravity potential due to the mantle can be evaluated directly by the Ferrers' ellipsoid with mantle density ρ_{mantle}. The potential due to the crust layer can be calculated by the potential due to the crustal polyhedron minus the one due to the core ellipsoid with mantle density (Takahashi and Scheeres 2014).

For the two-layered internal structure of Vesta, the assumption made by Parker et al. (2014) are followed that the crust layer owns a density variation of 2310-3440 kg/m^3 and 2660-3240 kg/m^3 for the 22.4 km and 55.5 km crustal

[5] The data to construct the polyhedral shape of Vesta can be found in Planetary Data System with the following link: https://sbn.psi.edu/pds/.

[6] JPL Small-body Database Browser.

thickness models. The mantle density ranges from 3400 kg/m^3 to 4400 kg/m^3 and the crustal density owns a range of 2000-3300 kg/m^3. Hence, the magnitude of a_{mantle} of the mantle ellipsoid is determined by the thickness of crust layer. Its ratio to the magnitude of b_{mantle} ranges from 0.6 to 0.95 so as the one of b_{mantle} to c_{mantle}. The physical parameters used in this investigation guarantees a total cover over the estimated range of Vesta's mass (2.22×10^{20} kg to 3.02×10^{20} kg) (Kattoum and Dombard 2009), as demonstrated by Fig. 2, where blue and orange region indicates the mass distribution for two- and three-layered structure.

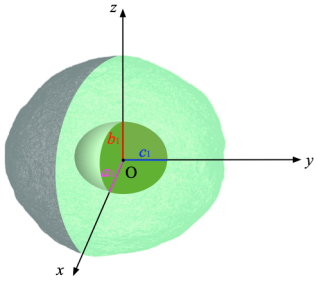

Fig. 1 A sketch of two-layered structure of Vesta.

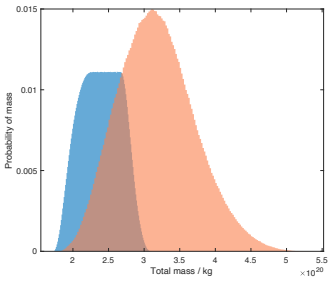

Fig. 2 Mass distribution.

2.2 Flying State Observation

According to Eq. (1) and Eq. (2), the flying trajectory of a spacecraft flying around Vesta is determined by the potential of Vesta body, which is parameterized by (ρ_{crust}, ρ_{core}, $a_{\text{core}}, b_{\text{core}}, c_{\text{core}}$) and ($\rho_{\text{crust}}$, ρ_{mantle}, ρ_{core}, a_{mantle} (b_{mantle}), c_{mantle}, a_{core} (b_{core}), c_{core}). Starting from a certain initial state $\boldsymbol{X}_{\text{initial}}$, the final state $\boldsymbol{X}_{\text{final}}$ after a fixed time T is obtained through numerically propagation but can not be explicitly expressed. Thus, once a mapping between the physical parameters of Vesta internal structure and the flying state of spacecraft is established successfully, the interior of Vesta can be predicted from the in-situ or reconstructed flying state observation without an ergodic and heavy computation. Such mapping and its inverse can be mathematically expressed as

$$\boldsymbol{\Phi}=\Gamma(\boldsymbol{X}_{\text{final}}(\boldsymbol{X}_{\text{initial}},T)) \quad \text{or} \quad \boldsymbol{X}_{\text{final}}(\boldsymbol{X}_{\text{initial}},T)=\Gamma^{-1}(\boldsymbol{\Phi}) \tag{7}$$

where $\boldsymbol{\Phi}$ denotes the physical parameter set of Phobos interior.

Flying state observations starting from planar and vertical Kepler orbits are used to build up the individual mapping Γ. Targeting at a two-layered internal structure, one generated from $\boldsymbol{X}_{\text{initial}}$=[589 km, 0, 0, 0, 171.3181 m/s, 0]^T and one generated from $\boldsymbol{X}_{\text{initial}}$=[0, 0, 589 km, 0, 171.3181 m/s, 0]^T are used. For a three-layered internal structure, the flying feedbacks are taken along the orbit generated from $\boldsymbol{X}_{\text{initial}}$=[889 km, 0, 0, 0, 139.4472 m/s, 0]^T and along the one generated from $\boldsymbol{X}_{\text{initial}}$=[0, 0, 889 km, 0, 139.4472 m/s, 0]^T. The nominal orbits in the polyhedron model of Vesta without core or mantle are illustrated in the body-fixed frame (O-x-y-z) and in the inertial frame (O-x_i-y_i-z_i), in Fig. 3(a) and Fig. 3(b), respectively. They share a similar altitude to Dawn spacecraft in low-orbit and high-orbit parking around Vesta (Konopliv et al. 2014). Because of the non-symmetric polyhedron shape of the Vesta body, the orbits generated from these two initial states are nearly-planar and nearly-vertical. This fact avoids singularity in mapping z or x and y coordinates to c or a and b of mantle and core ellipsoids but suggests that results based on nearly-planar and nearly-vertical orbits can work as two extreme cases examining the sensitivity of flying state observation to internal structure. To release computational burden, the final state $\boldsymbol{X}_{\text{final}}$ is recorded after a flying time of 1/4 of the period of the nominal orbit.

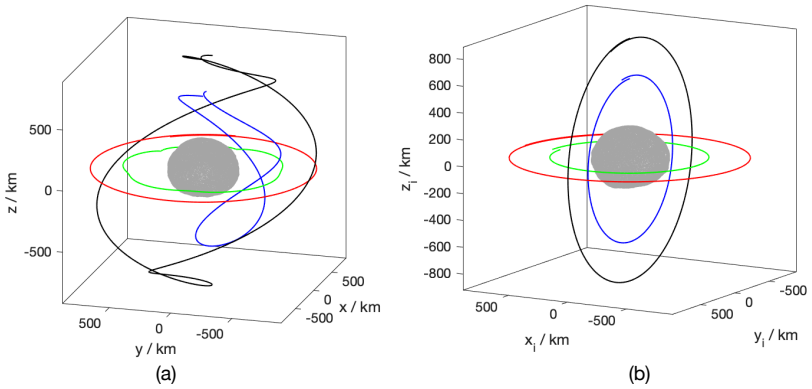

Fig. 3 Nominal nearly-planar and nearly-vertical orbits in the polyhedron model of Vesta: red and green lines indicate the low-altitude and high-altitude nearly-planar orbits; black and blue lines indicate the low-altitude and high-altitude nearly-vertical orbits.

3 Neural Network Setup

3.1 Training Evaluation

This invertible network offers the opportunity to simultaneously optimize the losses on both the in- and output domain (Grover et al. 2017). Thus, the success of this bi-directional training is evaluated by the following losses, i.e., the MMD loss in both forward and backward process comparing of two probability distributions through samples, the averaged loss of output and re-simulated $\boldsymbol{Y}$ and the averaged loss of input and re-constructed $\boldsymbol{X}$, to measure the accuracy of training for point estimations. The latter two losses are estimated as the root mean square error of each component with respect to the value obtained via training and denoted by $\text{Loss}^{\boldsymbol{X}}$ and $\text{Loss}^{\boldsymbol{Y}}$, respectively. These four losses are recorded after each iteration of training until they ultimately converge, which takes about 50-60 training iterations, as illustrated in Fig. 5. In this investigation, the INNS must be trained individually based on four astrodynamical and astrophysical assumptions based on four combination of nominal orbits and interior structure, i.e., a low-altitude nearly-planar orbit in a two-layered structure denoted by LP2L. its convergence process estimated by the aforementioned losses is illustrated in Fig. 5, respectively.

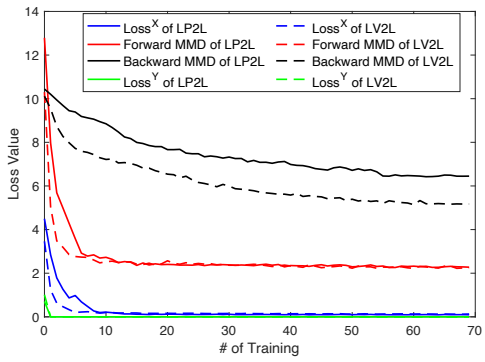

Fig. 5 Convergence process estimated by four losses in LP2L and LV2L case.

4 Prediction Performances

In the environment of macOS Big Sur system with an Apple M1 chip taking advantage of GPU acceleration, training the INNs until convergence for the LP2L and LV2L cases costs about 2.67 to 3.41 hours. Testing the well-trained INNs model for prediction is much faster based on a dataset of 20000 samples. A total test of 2000 times on each data consumes about 30 minutes. The final goal of this investigation is to develop a method predicting the internal structure of a target

body using flying data, so the testing performances are evaluated through a comparison of true value of sample physical parameter data and reconstructed data for 20000×2000 tests. To access the limitations of the method based on different nominal orbits and assumed internal structure, a case-dependent analysis based on the current numerical results is conducted as follows.

Fig. 8 illustrates the correlation of sample and reconstructed physical parameters and the error distribution at each true value by the counts density. The plot highlights how well the INN predicts ρ_{crust}, ρ_{mantle}, a_{mantle}, b_{mantle}, and c_{mantle} for all tests. Most of the predictions locate on a perfect 1-to-1 correlation between the reconstructed and true values, as demonstrated by Fig. 7(a), 7(c), 7(e), 7(g), and 7(i), respectively. Despite the generally satisfactory match, local slight blemish appears within some ranges for specific physical parameters, which is presented by the error distribution of Fig. 7(b), 7(d), 7(f), 7(h), and 7(j). The correlation plots for both a_{mantle} and b_{mantle} show the neck regions at specific range of true value, indicating uneven prediction performances along these two parameters. In particular, the smaller error distribution happens as the semi-axis of the mantle ellipsoid a_{mantle} ranges from 235 km to 245 km, corresponding to a crust height of about 53 km – 71 km based on polyhedron shape of Vesta body. Still, in the rest ranges, there is a majority of good predictions. The dramatic change of prediction performances near the neck region is presented in details by taking three slices taken from Fig. 7(f) as the true value of a_{mantle}=240 km, 244 km, and 250 km, as shown in the probability distribution of Fig. 8(b). Along the reasonable range of b_{mantle} occurs two neck regions with smaller standard deviation, i.e., 138 km – 148 km and 190 km – 210 km. Particularly, three slices are taken near the right neck region at true values of b_{mantle}=182 km, 192 km, and 207 km with their probability distribution shown in Fig. 8(c).

As the flying state is feedbacked from a nearly-planar nominal orbit, it is supposed that the motion along *z*-axis can not be perturbed as strongly as planar motion by the potential change due to the various size of the plane symmetric mantle ellipsoids despite the non-symmetric polyhedron shape of Vesta body. Thus, the largest scatter is assumed to occur in the c_{mantle} prediction of the mantle ellipsoid, which matches the numerical results shown in Fig. 7(j) and the probability distribution at the true value of c_{mantle}=100 km in Fig. 8(d).

Conclusions

This investigation is devoted to the development of an interdisciplinary method to predict the internal structure of asteroids, combining knowledges of astrophysics, astrodynamics, and data science. In particular, a data-driven approach called Invertible Neural Networks (INNs) is introduced for the inverse problem "reading" the density distribution of a differentiated asteroid conditioned on a specific flying state of a spacecraft directly. A multiple-layered model is used to describe the heterogeneous density distribution of the differentiated asteroids. Flying states are taken as the observation along four different nominal orbits, which are generated from the similar altitude of parking orbits in Dawn mission in planar and vertical plane, respectively. Based on the parameters of Vesta, the training and testing performances of INNs are evaluated in the case of, i.e., low-altitude nearly-planar trajectory in 2-layered model (LP2L). Finally, it is noticed that this data-based method is applicable for other fully or partially differentiated asteroids like Ceres or Lutetia in a similar manner and can be extended to other types of small bodies or moons like Phobos if their density distribution is parameterized within the computation allowance using proper flying state observation.

References

Scheinberg A, Fu R R, Elkins-Tanton L T, et al. Asteroid differentiation: Melting and large-scale structure[J]. Asteroids IV, 2015: 533-552.

Thomas P C, Parker J W, McFadden L A, et al. Differentiation of the asteroid Ceres as revealed by its shape[J]. Nature, 2005, 437(7056): 224-226.

Zuber M T, McSween H Y, Binzel R P, et al. Origin, internal structure and evolution of 4 Vesta[J]. Space science reviews, 2011, 163(1): 77-93.

Neumann W, Breuer D, Spohn T. The thermo-chemical evolution of Asteroid 21 Lutetia[J]. Icarus, 2013, 224(1): 126-143.

Neumann W, Henke S, Breuer D, et al. Modeling the evolution of the parent body of acapulcoites and lodranites: A case study for partially differentiated asteroids[J]. Icarus, 2018, 311: 146-169.

Park R S, Konopliv A S, Asmar S W, et al. Gravity field expansion in ellipsoidal harmonic and polyhedral internal representations applied to Vesta[J]. Icarus, 2014, 240: 118-132.

Kattoum Y N, Dombard A J. Calculating the topography of a differentiated Vesta[J]. Geophysical research letters, 2009, 36(24).

Ferrers, N. M., "On the Potentials, Ellipsoids, Ellipsoidal Shells, Elliptic Laminae, and Elliptic Rings of Variable Densities," *Quarterly Journal of Pure and Applied Mathematics*, Vol. 14, 1877, pp. 1-22.

Bellerose, J., Scheeres, D. J., "Stability of Equilibrium Points in the Restricted Full Three-body Problem," *Acta Astronautica*, Vol. 60, No. 3, 2007, pp. 141-152.
https://doi.org/10.1016/j.actaastro.2006.07.009

Gómez, M. R., "The role of invariant manifolds in the formation of spiral arms and rings in barred galaxies," Ph.D. Dissertation, Universitat Politècnica de Catalunya (UPC), Spain, 2007.

Liang, Y., Gómez, G., Masdemont, J. J., Xu, M., "Stable Regions of Motion Around a Binary Asteroid System," *Journal of Guidance, Control, and Dynamics*, Vol. 42, No. 11, 2019, pp. 2521-2531.
https://doi.org/10.2514/1.G004217

Takahashi Y, Scheeres D J. Morphology driven density distribution estimation for small bodies[J]. Icarus, 2014, 233: 179-193.

Werner, R. A., and Scheeres, D. J., "Exterior gravitation of a polyhedron derived and compared with harmonic and mascon gravitation representations of asteroid 4769 Castalia," *Celestial Mechanics and Dynamical Astronomy*, Vol. 65, No. 3, 1996, pp. 313-344. https://doi.org/10.1007/BF00053511

Luo Y, Yang Z. A review of uncertainty propagation in orbital mechanics[J]. Progress in Aerospace Sciences, 2017, 89: 23-39.

Aljbaae S, Chanut T G G, Carruba V, et al. The dynamical environment of asteroid 21 Lutetia according to different internal models[J]. Monthly Notices of the Royal Astronomical Society, 2017, 464(3): 3552-3560.

Russell C T, Raymond C A, Coradini A, et al. Dawn at Vesta: Testing the protoplanetary paradigm[J]. Science, 2012, 336(6082): 684-686.

Konopliv A S, Asmar S W, Park R S, et al. The Vesta gravity field, spin pole and rotation period, landmark positions, and ephemeris from the Dawn tracking and optical data[J]. Icarus, 2014, 240: 103-117.

Park R S, Konopliv A S, Asmar S W, et al. Gravity field expansion in ellipsoidal harmonic and polyhedral internal representations applied to Vesta[J]. Icarus, 2014, 240: 118-132.

Ermakov A I, Zuber M T, Smith D E, et al. Constraints on Vesta's interior structure using gravity and shape models from the Dawn mission[J]. Icarus, 2014, 240: 146-160.

Ardizzone L., Kruse J., Rother C., KÃüthe U., 2019a, in International Conference on Learning Representations. https://openreview.net/forum?id=rJed6j0cKX

Ardizzone L., Lüth C., Kruse J., Rother C., Köthe U., 2019b, CoRR, abs/1907.02392.

Ksoll V F, Ardizzone L, Klessen R, et al. Stellar parameter determination from photometry using invertible neural networks[J]. Monthly Notices of the Royal Astronomical Society, 2020, 499(4): 5447-5485.

Dinh L., Sohl-Dickstein J., Bengio S., 2016, arXiv e-prints, p.arXiv:1605.08803.

Ilya Tolstikhin, Olivier Bousquet, Sylvain Gelly, and Bernhard Schoelkopf. Wasserstein auto-encoders. arXiv:1711.01558, 2017.

Hyvärinen A, Oja E. Independent component analysis: algorithms and applications[J]. Neural networks, 2000, 13(4-5): 411-430.

Grover A, Dhar M, Ermon S. Flow-gan: Combining maximum likelihood and adversarial learning in generative models[C]//Thirty second AAAI conference on artificial intelligence. 2018.

Murray C D, Dermott S F. Solar system dynamics[M]. Cambridge university press, 1999, chap. 1.3.

Kanamaru M, Sasaki S, Wieczorek M. Density distribution of asteroid 25143 Itokawa based on smooth terrain shape[J]. Planetary and Space Science, 2019, 174: 32-42.

Rosenblatt P. The origin of the Martian moons revisited[J]. The Astronomy and Astrophysics Review, 2011, 19(1): 1-26.

Takahashi Y, Scheeres D J. Morphology driven density distribution estimation for small bodies[J]. Icarus, 2014, 233: 179-193.